

A training-free recursive multiresolution framework for diffeomorphic deformable image registration

Ameneh Sheikhjafari^{1,3*}, Michelle Noga^{2,3}, Kumaradevan Punithakumar^{2,3**},
and Nilanjan Ray^{1**}

¹ Department of Computing Science, University of Alberta, Canada

² Radiology and Diagnostic Imaging, University of Alberta, Canada

³ Servier Virtual Cardiac Centre, Mazankowski Alberta Heart Institute, Canada

*Corresponding author. E-mail: sheikhja@ualberta.ca

Contributing authors: mnoga@ualberta.ca, punithak@ualberta.ca, nray1@ualberta.ca

**These authors contributed equally to this work.

Abstract. Diffeomorphic deformable image registration is one of the crucial tasks in medical image analysis, which aims to find a unique transformation while preserving the topology and invertibility of the transformation. Deep convolutional neural networks (CNNs) have yielded well-suited approaches for image registration by learning the transformation priors from a large dataset. The improvement in the performance of these methods is related to their ability to learn information from several sample medical images that are difficult to obtain and bias the framework to the specific domain of data. In this paper, we propose a novel diffeomorphic training-free approach; this is built upon the principle of an ordinary differential equation.

Our formulation yields an Euler integration type recursive scheme to estimate the changes of spatial transformations between the fixed and the moving image pyramids at different resolutions. The proposed architecture is simple in design. The moving image is warped successively at each resolution and finally aligned to the fixed image; this procedure is recursive in a way that at each resolution, a fully convolutional network (FCN) models a progressive change of deformation for the current warped image. The entire system is end-to-end and optimized for each pair of images from scratch. In comparison to learning-based methods, the proposed method neither requires a dedicated training set nor suffers from any training bias. We evaluate our method on three cardiac image datasets. The evaluation results demonstrate that the proposed method achieves state-of-the-art registration accuracy while maintaining desirable diffeomorphic properties.

Keywords: Diffeomorphic registration · Multiresolution deformable image registration · Euler integration · Convolutional neural network.

1 Introduction

Deformable image registration is an important part of a variety of medical image processing applications. For instance, deformable registration is applied for the quantification of regional function measures and tracking heart motion [12,24] in cardiology. The aim of the deformable image registration is to establish a point-wise correspondence between two images to align them by estimating an appropriate non-linear transformation.

There is a strong need for the development of accurate and reliable nonrigid registration algorithms for many medical imaging applications. Many deformable registration algorithms have been proposed by various research groups and existing algorithms could be broadly categorized into non-learning-based (classical) methods and learning-based methods.

Commonly, non-learning-based registration techniques solve regularized optimization problems using an image similarity/dissimilarity metric and regularization. These methods include nonlinear elastic-based methods [6], diffusion-based methods [15], B-splines [17,26], demons algorithm [16], diffeomorphic transformation-based methods [1,15,20]. Adapting the conventional methods to specific problems is challenging, as they require a precise model parameterization that can be too flexible or too restrictive. Besides, occasionally regularization terms need to be manually adjusted for each application to obtain accurate results. However, recent studies show that the regularization prior can be modeled by neural networks, independent of learning, for deformable image registration [14,25] to remove the need for manual adjustment of parameters.

In the past few years, learning-based approaches, notably deep CNNs, have been successfully applied in different computer vision problems such as color enhancement, color compensation, and image registration [28,29,30,31,32]. In supervised-learning based image registration methods, CNN is trained using examples of medical images along with their ground truth transformations to predict the transformations directly on test images [7,22,33]. Even though the accuracy of these approaches is considerable, their performance is bounded by the quality of the synthetic ground truth deformation field or the annotated map [23]. Additionally, the actual ground truth of a desired neural network output is not often available.

Unsupervised image registration methods have received a lot of attention because they bypass the need for annotated data. In addition, the quality of the output in unsupervised registration methods does not depend on the quality of labels. However, they are often trained on a set of images which could introduce bias on specific data. These methods utilize a CNN and a differentiable similarity function to learn the dense spatial mapping between input image pairs [3,28]. Also, it must be noted that most of the existing CNN-based methods often do not consider desirable diffeomorphic properties including invertibility and inverse consistency of the transformation [19].

In this paper, we propose a novel learning-free diffeomorphic recursive framework using an FCN capable of estimating plausible non-linear transformations between images. The main elements of this work are:

Algorithm 1: ODE-based Multi-resolution Diffeomorphism

Input: Pixel coordinates $\{X_t\}_{t=1}^K$ for all resolutions
Output: Deformation fields $\{D_t\}_{t=1}^K$ for all resolutions
-Initialize a spatial transformation
 $V_K = f_\theta(X_K, 0)$
 $D_K = EXP(V_K)$
for $t \leftarrow K - 1$ **to** 0 **do**
 $D_{t+1}^{up} = UpSample(D_{t+1})$
 $V_t = f_\theta(X_t, D_{t+1}^{up})$
 $V_t \leftarrow LowPass(V_t)$
 $D_t = D_{t+1}^{up} \circ EXP(V_t)$
end

1. In the proposed method, an FCN models *the changes* in the deformation over multiple resolutions as opposed to the deformation itself that most existing methods do. The final deformation is estimated by a solution to an ordinary differential equation (ODE). Thus the resulting algorithm is recursive in nature.
2. Following this recursion, the moving image is warped successively, enabling the final prediction, which might consist of large displacements, to be decomposed into smaller displacements.
3. Within the recursive algorithmic framework, we introduce diffeomorphism, which guarantees the inverse consistency of deformations.
4. The proposed method is learning-free, i.e., it optimizes the parameters of the FCN from scratch for every new pair of images and eliminates the need for a dedicated training set.
5. The parameters of the FCN are shared across all resolutions and the neural net loss function values at all resolutions are optimized simultaneously.

2 Methodology

Let $I_m \in \Omega$, $I_f \in \Omega$ denote the moving image and the fixed image respectively which are both defined over d-dimensional space Ω . D is the deformation field which maps $D : \Omega \rightarrow \Omega$. Commonly, deformable registration methods construct a deformation prediction function F which takes moving and fixed images as inputs and predicts a dense deformation field that aligns I_m to I_f . In contrast, in the proposed approach, we construct F as a function of coordinate grid (not images) to predict the the change in the deformation field from one resolution to the next resolution. We cascade this procedure by recursively performing registration on the multi-resolution levels. Following this recursion, the change of deformation field is predicted at each resolution, enabling the final deformation field probably with large displacement to be decomposed into cascade with small displacement.

In multi-resolution pyramids, a Gaussian pyramid of images is constructed where the original image lies at the bottom level and subsequently higher levels have a down-scaled Gaussian blurred version of the image. Multi-resolution pyramids often serve to accelerate the optimization and yield better accuracy. Using a multi-resolution recipe, two image pyramids are built: I_F^t and I_M^t for $t = K, \dots, 1$, where K is the maximum level in the pyramid. Here, $I_F^1 = I_F$ and $I_M^1 = I_M$ are the original fixed and moving images, respectively.

Considering resolution t as the continuous variable, the change in deformation over resolution t is conceived by a FCN f_θ :

$$\frac{d}{dt}D_t = f_\theta(X_t, D_t), \quad (1)$$

where X_t , a multi-dimensional array, is the pixel coordinate grid at resolution t and D_t is the deformation field, another multi-dimensional array at resolution t . Thus, we model the change in deformation as a function of both the coordinate grid and the deformation. Discretization of the resolution (i.e., pyramid levels) leads to a solution by a Euler integration with an initial value D_K :

$$D_t = D_{t+1} + f_\theta(X_{t+1}, D_{t+1}), \quad \text{for } t = K - 1, K - 2, \dots, 1, \quad (2)$$

where $t = K$ is the coarsest and $t = 1$ is the finest/original resolution. D_{t+1} is the upsampled deformation field from a lower level D_t and $f_\theta(D_{t+1})$ is the changes of the deformation field at resolution $t + 1$ from resolution t .

Additionally, to have the same canonical range of pixel coordinates at every resolution, in our implementation, we use the range $[-1, 1] \times [-1, 1]$ for pixel coordinates. With this view, a multi-resolution pyramid adds more samples in the space $[-1, 1] \times [-1, 1]$ as we go from lower to higher resolutions.

A reasonable deformation field should prevent folding and be continuously varying (diffeomorphism). By taking the composite form in the Euler integration instead of the additive form, we introduce diffeomorphism to the framework. Further, if we treat the output of the FCN as the velocity field, then exponential of the velocity field will yield the multi-resolution diffeomorphic deformation:

$$D_t = D_{t+1} \circ EXP(f_\theta(X_{t+1}, D_{t+1})), \quad \text{for } t = K - 1, K - 2, \dots, 1. \quad (3)$$

The computational scheme for (3) appears in Algorithm 1, where we introduced two more functionalities: upsampling and smoothing. Upsampling interpolates a deformation from a lower to the next upper level of resolution and smoothing of the velocity field acts as an implicit regularizer for image registration.

In this work, we use geometric optimization that uses the local canonical coordinates [27]. Based on this method, to estimate the current deformation, a compositional update rule is used between the previous estimate and the exponential map EXP of the displacement field. The exponential map is efficiently calculated by using the scaling and squaring method [10] and the composition of displacement fields. The exponentiation of the displacement field ensures the

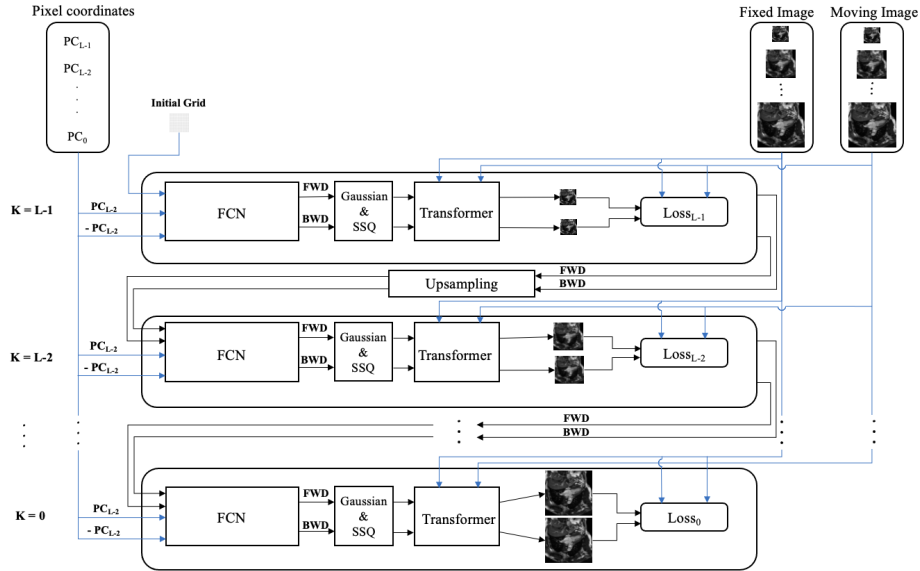


Fig. 1: Schematic of the proposed recursive algorithm. $PC_{K-1}, PC_{K-2}, \dots, PC_0$ are pixel coordinates correspond to the image pyramids. PC and $-PC$ are passed as the inputs to the network for forward and backward directions. An initial grid with zero displacement is used as a correction for the resolution $t = K - 1$. The outputs of the FCN, forward deformation field FWD and backward deformation field BWD will be smooth by a Gaussian filter and then passed to the scaling and squaring method SSQ . The final FWD and BWD generated at each resolution will be passed to an upsampler and then the upsampled results will be used as a correction for the next resolution. For each pair of images we repeat the whole process (e.g. 800 iterations) till we find the optimum value of θ

diffeomorphism of the mapping. Therefore, our recursive diffeomorphic image registration is obtained with Algorithm 1. Also the schematic of the proposed recursive algorithm is shown in 1. To optimize the FCN parameters θ , we use two Gaussian pyramids, one each for the moving I_M^t and the fixed I_F^t images, where $t = 1, \dots, K$. Then, the FCN's parameters will be optimized based on the difference between warped moving image and fixed image at the same resolution. In our approach, the neural network will be optimized from the scratch for each pair of images being registered, and therefore, the trainable parameter values of the network will at convergence will be different. Our approach is a classical learning-free setting which would not require a dedicated training set with annotations of any kind from experts.

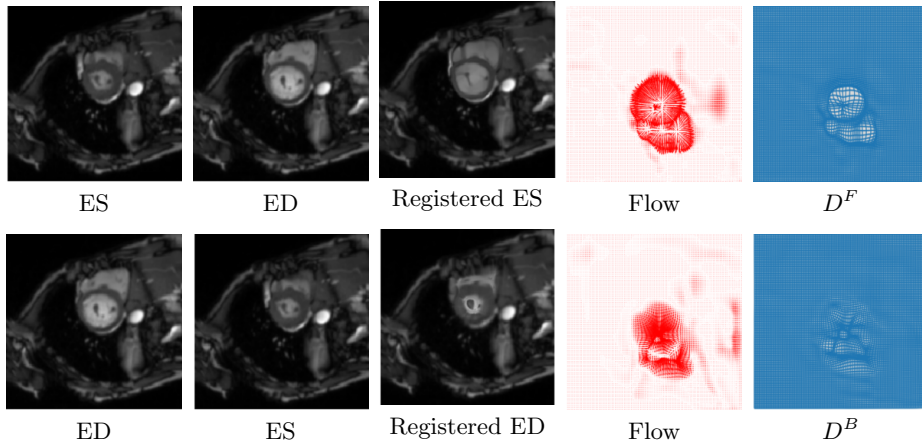


Fig. 2: A sample result of forward and backward registrations with velocity fields and grid deformation fields from ACDC dataset.

The parameters θ of the FCN are found by solving the following optimization using gradient descent (we use PyTorch’s autograd):

$$\min_{\theta} \sum_{t=1}^K \sum_{x \in \Omega} L(I_F^t(x), I_M^t(D_t(x))) + \gamma \|D_t(x) - x\|^2, \quad (4)$$

where Ω denotes the fixed and moving images domain, $I_F^t(x)$ is the fixed image pixel value at pixel location x and resolution level t . $I_M^t(D_t(x))$ in (4) refers to the pixel value on the moving image I_M^t at location x after being displaced by deformation field $D_t(x)$. $L(\cdot, \cdot)$ is a differentiable loss function. In order to use the same range of displacement for all levels of resolution, we normalized the deformation field and the index at all resolutions in a canonical range $[-1, 1]$.

In most of the learning-based deformable image registration approaches, the inverse mapping is often ignored [19]. However, the accuracy of the nonrigid registration could be improved by computing the mappings from moving to fixed image and vice versa as well as exploiting the invertible property of diffeomorphic transformations.

In the proposed registration framework, we employ a FCN with two dense velocity fields to generate two deformation fields, namely, forward D^F and backward D^B deformation fields, that register images I_M to I_F and I_F to I_M , respectively, using Algorithm 1. We then enforce the consistency constraint that these two transformations are inverse mappings of each other by adding a regularization term to the loss function. Our FCN architecture consists of 4 convolution layers, each contains twenty-four 5×5 filters with a stride of 1, followed by a rectified linear unit (ReLU) activation, except for the last layer.

Note that the output of the Algorithm 1 is $D_t = [D_t^F, D_t^B]$ in which D_t^F and D_t^B are forward and backward deformation fields, respectively, see Fig. 2 as an

example. With this view the following forward-backward optimization is used:

$$\min_{\theta} \sum_{t=1}^K \sum_{x \in \Omega} [L_1(I_F^t(x), I_M^t(D_t^F(x))) + L_1(I_M^t(x), I_F^t(D_t^B(x))) + \alpha L_2(D_t^B(D_t^F(x)), x) + \alpha L_2(D_t^F(D_t^B(x)), x) + \gamma \|D_t^F(x) - x\|^2 + \gamma \|D_t^B(x) - x\|^2] \quad (5)$$

We use differentiable mutual information (MI) [4] and structural similarity index metric (SSIM) [4] as similarity metric $L_1 = MI + SSIM$ and mean squared error (MSE) as penalizes term to enforce the inverse consistency $L_2 = MSE$.

Table 1: Quantitative evaluation of the results for cardiac MRI registration on the ACDC, SCD and LA datasets. The evaluation was performed in terms of Dice (mean± standard deviation) and HD (mean) and the average number of pixels with non-positive Jacobian Determinant (lower is better). Values in bold indicate the best performance.

Methods	ACDC			SCD		
	Dice	HD	det(J_ϕ) < 0	Dice	HD	det(J_ϕ) < 0
Unregistered	0.65 ± 0.20	17.76	N/A	0.62 ± 0.15	N/A	N/A
RTT(L2L2)	0.76 ± 0.18	7.19	0.10	0.70 ± 0.12	5.36	0.30
RTT(L2L1)	0.78 ± 0.18	6.64	0.25	0.70 ± 0.12	5.36	0.30
Elastix	0.79 ± 0.18	11.26	0.32	0.79 ± 0.08	N/A	0.37
LCC-D*	0.79 ± N/A	9.21	N/A	-	-	-
VM*	0.79 ± N/A	8.46	N/A	-	-	-
LVM (S1)*	0.79 ± N/A	7.58	N/A	-	-	-
SyN*	0.80 ± N/A	8.24	N/A	0.81 ± 0.16	8.9	0.02
MM	0.81 ± 0.18	8.59	0	0.72 ± 0.12	3.48	0
LVM (S3)*	0.81 ± N/A	6.88	N/A	-	-	-
Demons	-	-	-	0.65 ± 0.18	15.46	0.42
DIRNet**	-	-	-	0.80 ± 0.08	N/A	N/A
Ours	0.92 ± 0.10	4.76	0	0.85 ± 0.15	5.06	0

Methods	LA								
	Dice			HD			det(J_ϕ) < 0		
	2ch	3ch	4ch	2ch	3ch	4ch	2ch	3ch	4ch
Unregistered	0.79 ± 0.07	0.78 ± 0.08	0.78 ± 0.09	7.37	7.70	8.66	N/A	N/A	N/A
Elastix	0.81 ± 0.13	0.86 ± 0.08	0.80 ± 0.11	7.9	6.99	8.01	0.68	0.5	0.75
RTT	0.82 ± 0.11	0.85 ± 0.10	0.80 ± 0.10	7.28	6.82	7.56	0.53	0.45	0.7
MM	0.84 ± 0.06	0.83 ± 0.06	0.83 ± 0.08	6.58	6.48	6.77	0.01	0	0
Demons	0.84 ± 0.08	0.85 ± 0.06	0.82 ± 0.10	7.41	7.33	7.84	0.025	0.042	0
SyN	0.87 ± 0.06	0.86 ± 0.13	0.84 ± 0.11	6.92	7.52	7.51	0.033	0	0.01
Ours	0.89 ± 0.11	0.92 ± 0.06	0.86 ± 0.11	6.26	5.7	7.44	0	0	0

*Results are reported in [13]. **Results are reported in [28]. N/A refers to the value that are not reported in the original paper.

3 Experiments

Data: The proposed framework is evaluated on three clinical cardiac MRI datasets: 1) Automated Cardiac Diagnosis Challenge (ACDC) dataset [5] which contains MRI scans including 100 stack of short-axis cardiac cine MRI sequences, each consisting of 12 to 35 temporal frames. 2) SunnyBrook cardiac dataset (SCD) [21] which contains 45 cardiac cine MRI scans each with 20 temporal frames. 3) Left atrium (LA) from the 2-chamber (2ch), 3-chamber (3ch) and 4-chamber (4ch) cine long-axis MRI sequences acquired retrospectively at our center that consists of 120 pairs of images in each chamber group. In all three datasets, we applied the proposed framework on end-diastole (ED) and end-systole (ES) cardiac frames from the cine sequences.

Implementation: The proposed method is implemented in Python programming language using Pytorch module. In neural network design, the Adam optimization with 800 update iterations and a learning rate of 5×10^{-4} are used for all the three datasets. The level of pyramid K is considered 2 with $\alpha = 1/(K)$, $\gamma = \frac{\lambda \times 1}{K}$, $\lambda = 5$. The neural net framework is evaluated on an NVIDIA GeForce GTX 1080 Ti GPU.

Evaluation Metrics: The Dice metric (DM), reliability, Hausdorff distance (HD) and the determinant of Jacobian are used as the evaluation metrics to compare the performance of the algorithms.

Dice Metric The DM [9] is a well-known segmentation based metric to measure the similarity (overlap) between two regions, warped moving and fixed image. The DM of two regions A and B is formulated as:

$$DM(A, B) = \frac{2|A \cap B|}{A + B} \quad (6)$$

Reliability The algorithms are examined by evaluating the reliability function [2] of the obtained DMs using (7). The complementary cumulative distribution function is defined for each $d \in [0, 1]$ as the probability of obtaining DM higher than d over the entire set. The $R(d)$ measures how reliable is the algorithm in yielding accuracy d .

$$R(d) = P_r(Dice > d) = \frac{\# \text{ Images segmented with DM higher than } d}{\text{total number of images}} \quad (7)$$

Hausdorff Distance The HD [11] is another well-known metric which measures the maximum deviation between two regions' contours. The HD between two contours (C_A) and C_B is formulated as:

$$HD(C_A, C_B) = \max(\max_i(\min_j(d(p_A^i, p_B^j))), \max_j(\min_i(d(p_A^i, p_B^j)))) \quad (8)$$

where p_A^i, p_B^j denote the set of all the points in C_A and C_B respectively. The term $d(\cdot)$ denotes the Euclidean distance.

Table 2: Quantitative cardiac MRI registration results on 50% patients of ACDC, SCD and LA datasets based on different loss functions. The evaluation was performed in terms of average Dice, HD and the forward and backward registration time (per second).

SCD				ACDC			
Methods	Dice	HD	Time(s)	Methods	Dice	HD	Time(s)
MSE	0.83	9.1	15	MSE	0.87	5.73	15
SSIM	0.86	7.9	20	SSIM	0.92	4.31	21
SSIM + MI	0.89	6.01	26	SSIM + MI	0.93	4.31	35

LA							
Methods	Dice			HD			Time (s)
	2ch	3ch	4ch	2ch	3ch	4ch	
MSE	0.84	0.86	0.84	6.83	6.88	7.84	15
SSIM	0.91	0.93	0.89	6.26	6.11	6.42	22
SSIM + MI	0.90	0.93	0.87	6.89	5.22	6.40	35

Determinant of Jacobian We quantify and analyze deformation regularity using the determinant of the Jacobian, $\det(J_\phi)$. Jacobian matrix captures the local behaviours of the deformation field. If the value of $\det(J)$ equals to 1, the volume remains constant after the transformation, the value smaller than 1 shows the local volume shrinkage and greater than 1 shows the local volume expansion. The negative values imply that local folding and twists have occurred, which is physically not realizable and mathematically not inevitable [8].

3.1 Evaluation Results and Discussions

The performance of the proposed framework is compared with nine state-of-the-art learning-based and classic deformable registration algorithms including SimpleElastix (Elastix) [17], Moving Mesh (MM) [20], Real-Time Image-based Tracker (RTT) [34], Demons [18], LCC-Demons (LCC-D) [15], Symmetric Normalization (SYN) [1], [8], [13] and DIRNet [28].

Table 1, shows the mean and standard deviations of Dice scores, HD and the average number of pixels with non-positive $\det(J_\phi)$ over all subjects ACDC, SCD, and left atrium datasets. Compared to the conventional and learning-based methods, our framework has the best performances in terms of Dice scores. In Fig. 4, the highest accuracy, 50th percentile, and the lowest accuracy in terms of Dice scores achieved by the proposed method are shown visually, where the red, blue, violet, gray and orange contours depict the correspondence segmentation results by the proposed method, RRT1, RRT2, Elastix and MM, respectively and the green contours depict the ground truth.

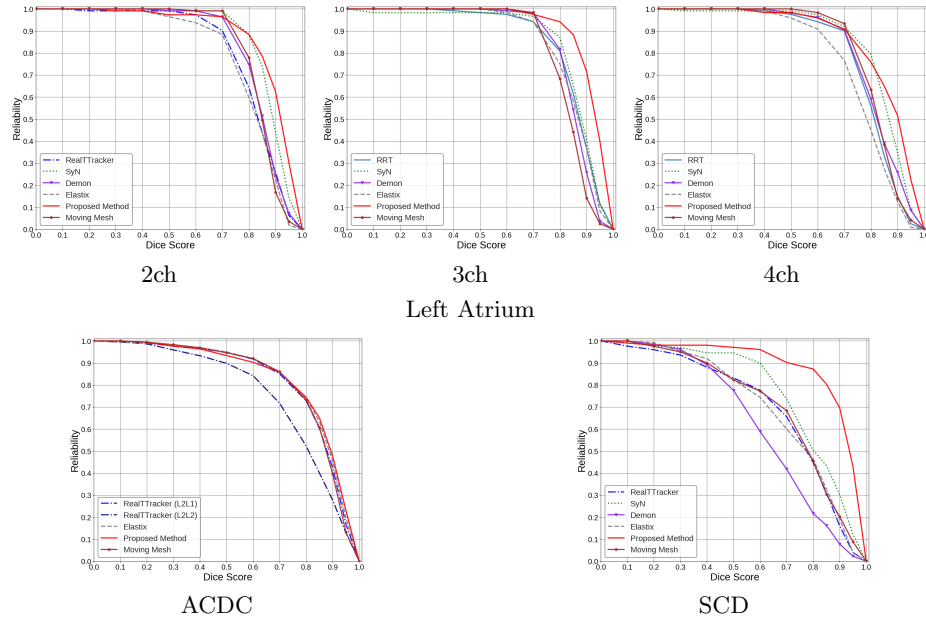


Fig. 3: Reliability versus Dice metric for different algorithms. The figures omit results for methods with no public implementation available.

To quantify and analyse deformation regularity, we computed the determinant of the Jacobian $\det(J_\phi)$ using SimpleITK [18]. No negative values of $\det(J)$ are observed for the proposed method as can be seen in Table 1.

We also evaluated the performance of the proposed algorithm in terms of the reliability function $R(d)$ [2]. The corresponding $R(d)$ are plot as a function of Dice score in Fig. 3. Our algorithm led to a higher reliability curve on all ACDC, SCD, and left atrium datasets.

We examined different loss functions, namely, MSE, SSIM and SSIM + MI, in our framework and reported the average time to register one pair of images (Computing both forward and backward deformation fields) as well as the average of DM and HD over 50% of patient datasets in Table 2. It can be seen that the MSE loss function led to the best average time; however, it does not yield the best accuracy in terms of the Dice score.

We assessed the impact of using different multi-resolution structures on the performance, and reported the corresponding evaluations in terms of DM and HD in Table 3. The results indicate that the high performance is obtained with the use of two resolutions.

Examples of registered images from ACDC, SCD, and left atrium datasets with their corresponding grid deformation are shown in Fig. 5 (a), (b), and (c), respectively. Fig. 5 shows the original ED, ES and their correspondence registered images and grid forward and backward deformations over images. The algorithm

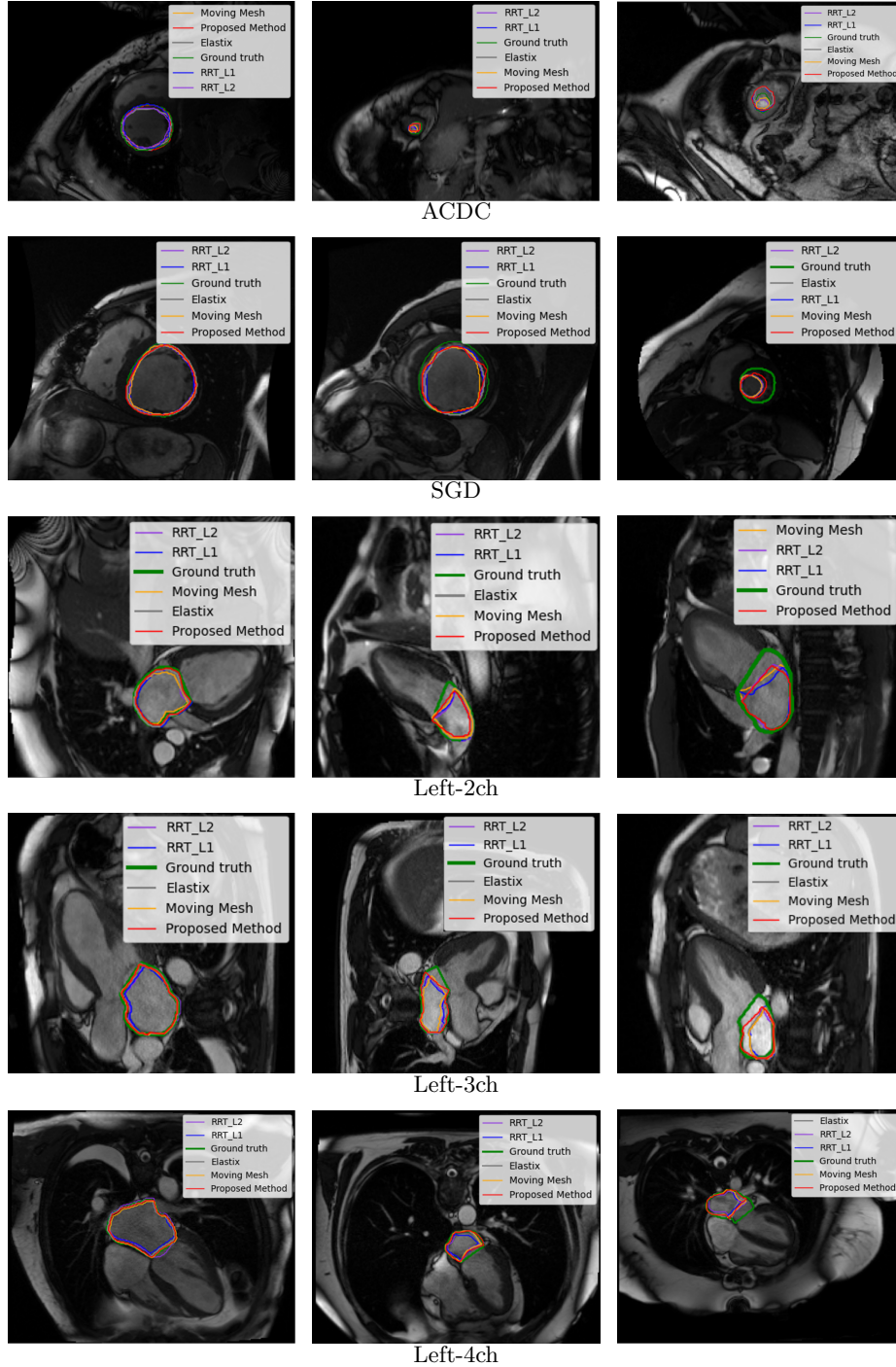


Fig. 4: The segmentation results with the highest (first column), 50th percentile (2nd column), lowest (3rd column) Dice score values for (a) ACDC (1st row), (b) SGD (2nd row), and left atrium (c) 2-chamber (3rd row), (d) 3-chamber (4th row), 4-chamber (5th row) views. The green represent the ground truth, also the red, blue, violet, gray and orange contours represent the boundary corresponds to the registration by proposed method, RRT1, RRT2, Elastix and MM, respectively

Table 3: Quantitative cardiac MRI registration results on the ACDC, SCD and LA based on different number of resolution. The evaluation is performed in terms of Dice (mean \pm standard deviation) and HD (mean). The 2ch, 3ch and 4ch stand for the 2, 3 and 4-chamber. Values in bold indicate the best performance.

	Dataset	Dice	HD
One Resolution	ACDC	0.85 ± 0.20	6.03
	SCD	0.85 ± 0.17	7.70
	LA-2ch	0.87 ± 0.08	7.6
	LA-3ch	0.91 ± 0.05	6.59
	LA-	0.88 ± 0.10	6.63
Two Resolutions	ACDC	0.87 ± 0.17	6.27
	SCD	0.86 ± 0.16	7.06
	LA-2ch	0.89 ± 0.09	7.59
	LA-3ch	0.93 ± 0.03	5.47
	LA-4ch	0.87 ± 0.11	6.67
Three Resolutions	ACDC	0.83 ± 0.22	6.70
	SCD	0.85 ± 0.18	7.22
	LA-2ch	0.86 ± 0.09	7.03
	LA-3ch	0.90 ± 0.06	6.22
	LA-4ch	0.86 ± 0.11	6.42
Four Resolutions	ACDC	0.74 ± 0.24	8.96
	SCD	0.85 ± 0.19	7.50
	LA-2ch	0.82 ± 0.10	7.06
	LA-3ch	0.86 ± 0.07	6.93
	LA-4ch	0.81 ± 0.10	7.01

is applied on whole images; however, to display the deformation tracking on the part that has the most changes, we cropped the grid.

We have also evaluated the outputs from the forward deformation field by ignoring the bidirectional registration to present its effects on the Dice score and HD. The forward deformation field yields Dice score values of 0.88 ± 0.17 and 0.87 ± 0.14 and HD values of 6.08 and 5.19 for ACDC and SCD, respectively, while the proposed bidirectional approach yields Dice score values of 0.92 ± 0.10 and 0.90 ± 0.15 and HD values of 4.76 and 5.06 for ACDC and SCD, as reported in Table 1. This clearly indicates the importance of including the bidirectional registration to obtain high performance.

4 Conclusion

We present an ODE-based diffeomorphic recursive framework for multi-resolution deformable registration using a FCN, to estimate the change velocity of forward

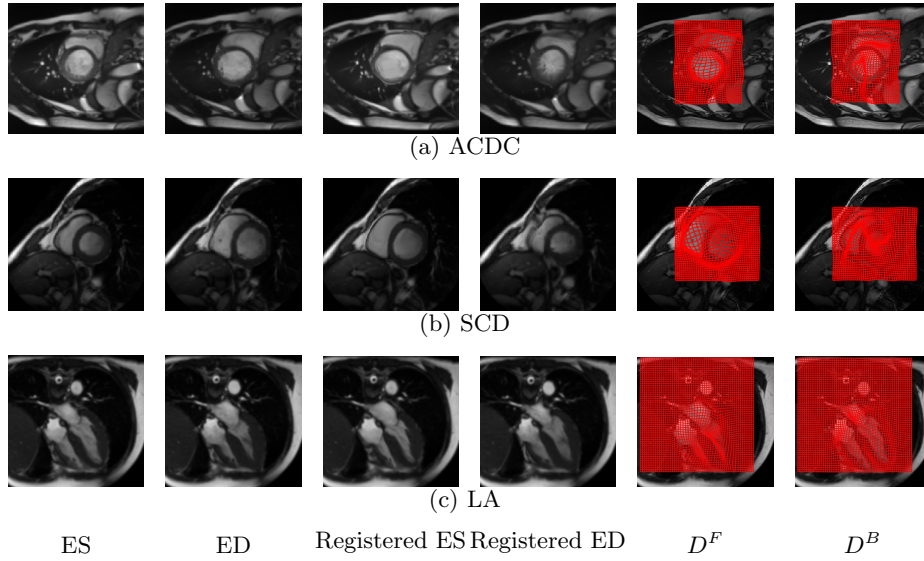


Fig. 5: Examples of pair images ES and ED from (a) ACDC, (b) SCD and (c) LA. Each row shows forward and backward registered images and the corresponding grid deformations. The registrations are applied to the whole image, however, the grids are cropped to have a better resolution

and backward deformation fields. We have then utilized inverse consistency loss to further guarantee the desirable diffeomorphic properties of the resulting solutions. The proposed framework is learning-free and does not require a dedicated training set.

The proposed approach simultaneously estimates the forward and backward mapping at all levels of the multi-resolution pyramid. We evaluated and compared the method using three different MRI datasets against several state-of-the-art traditional and learning-based registration methods. The results demonstrate that our method outperforms both traditional and learning-based methods.

References

1. Avants, B.B., Epstein, C.L., Grossman, M., Gee, J.C.: Symmetric diffeomorphic image registration with cross-correlation: evaluating automated labeling of elderly and neurodegenerative brain. *Medical Image Analysis* **12**(1), 26–41 (2008)
2. Ayed, I.B., Punithakumar, K., Li, S., Islam, A., Chong, J.: Left ventricle segmentation via graph cut distribution matching. In: *International conference on medical image computing and computer-assisted intervention*. pp. 901–909. Springer (2009)
3. Balakrishnan, G., Zhao, A., Sabuncu, M.R., Guttag, J., Dalca, A.V.: An unsupervised learning model for deformable medical image registration. In: *Proceedings of the IEEE conference on computer vision and pattern recognition*. pp. 9252–9260 (2018)

4. Belghazi, M.I., Baratin, A., Rajeswar, S., Ozair, S., Bengio, Y., Courville, A., Hjelm, R.D.: Mine: mutual information neural estimation. arXiv preprint arXiv:1801.04062 (2018)
5. Bernard, O., Lalande, A., Zotti, C., Cervenansky, F., Yang, X., Heng, P.A., Cetin, I., Lekadir, K., Camara, O., Ballester, M.A.G., et al.: Deep learning techniques for automatic **MRI** cardiac multi-structures segmentation and diagnosis: Is the problem solved? *IEEE transactions on medical imaging* **37**(11), 2514–2525 (2018)
6. Burger, M., Modersitzki, J., Ruthotto, L.: A hyperelastic regularization energy for image registration. *SIAM Journal on Scientific Computing* **35**(1), B132–B148 (2013)
7. Cao, X., Yang, J., Zhang, J., Wang, Q., Yap, P.T., Shen, D.: Deformable image registration using a cue-aware deep regression network. *IEEE Transactions on Biomedical Engineering* **65**(9), 1900–1911 (2018)
8. Dalca, A.V., Balakrishnan, G., Guttag, J., Sabuncu, M.R.: Unsupervised learning for fast probabilistic diffeomorphic registration. In: *International Conference on Medical Image Computing and Computer-Assisted Intervention*. pp. 729–738. Springer (2018)
9. Dice, L.R.: Measures of the amount of ecologic association between species. *Ecology* **26**(3), 297–302 (1945)
10. Higham, N.J.: The scaling and squaring method for the matrix exponential revisited. *SIAM review* **51**(4), 747–764 (2009)
11. Huttenlocher, D.P., Klanderman, G.A., Rucklidge, W.J.: Comparing images using the **hausdorff** distance. *IEEE Transactions on pattern analysis and machine intelligence* **15**(9), 850–863 (1993)
12. Khalil, A., Ng, S.C., Liew, Y.M., Lai, K.W.: An overview on image registration techniques for cardiac diagnosis and treatment. *Cardiology research and practice* **2018** (2018)
13. Krebs, J., e Delingette, H., Mailhé, B., Ayache, N., Mansi, T.: Learning a probabilistic model for diffeomorphic registration. *IEEE transactions on medical imaging* (2019)
14. Laves, M.H., Ihler, S., Ortmaier, T.: Deformable medical image registration using a randomly-initialized cnn as regularization prior. arXiv preprint arXiv:1908.00788 (2019)
15. Lorenzi, M., Ayache, N., Frisoni, G.B., Pennec, X., (ADNI, A.D.N.I., et al.: LCC-Demons: a robust and accurate symmetric diffeomorphic registration algorithm. *NeuroImage* **81**, 470–483 (2013)
16. Mansi, T., Pennec, X., Sermesant, M., Delingette, H., Ayache, N.: iLogDemons: A demons-based registration algorithm for tracking incompressible elastic biological tissues. *International journal of computer vision* **92**(1), 92–111 (2011)
17. Marstal, K., Berendsen, F., Staring, M., Klein, S.: SimpleElastix: A user-friendly, multi-lingual library for medical image registration. In: *Proceedings of the IEEE conference on computer vision and pattern recognition workshops*. pp. 134–142 (2016)
18. McCormick, M.M., Liu, X., Ibanez, L., Jomier, J., Marion, C.: ITK: enabling reproducible research and open science. *Frontiers in neuroinformatics* **8**, 13 (2014)
19. Mok, T.C., Chung, A.: Fast symmetric diffeomorphic image registration with convolutional neural networks. In: *Proceedings of the IEEE/CVF conference on computer vision and pattern recognition*. pp. 4644–4653 (2020)
20. Punithakumar, K., Boulanger, P., Noga, M.: A GPU-accelerated deformable image registration algorithm with applications to right ventricular segmentation. *IEEE Access* **5**, 20374–20382 (2017)

21. Radau, P., Lu, Y., Connelly, K., Paul, G., Dick, A., Wright, G.: Evaluation framework for algorithms segmenting short axis cardiac **MRI**. The MIDAS Journal-Cardiac MR Left Ventricle Segmentation Challenge **49** (2009)
22. Rohé, M.M., Datar, M., Heimann, T., Sermesant, M., Pennec, X.: SVF-Net: Learning deformable image registration using shape matching. In: International Conference on Medical Image Computing and Computer-Assisted Intervention. pp. 266–274. Springer (2017)
23. Sang, Y., Xing, X., Wu, Y., Ruan, D.: Imposing implicit feasibility constraints on deformable image registration using a statistical generative model. In: Medical Imaging 2020: Image Processing. vol. 11313, p. 113132V. International Society for Optics and Photonics (2020)
24. Sheikhsafari, A., Talebi, H.A., Zareinejad, M.: Robust and efficient **3d** motion tracking in robotic assisted beating heart surgery. In: 2015 IEEE International Conference on Robotics and Biomimetics (ROBIO). pp. 1828–1833. IEEE (2015)
25. Sheikhsafari, A., Noga, M., Punithakumar, K., Ray, N.: Unsupervised deformable image registration with fully connected generative neural network. In: Medical Imaging with Deep Learning (2018)
26. Sheikhsafari, A., Talebi, H., Zareinejad, M.: **3D** visual stabilization for robotic-assisted beating heart surgery using a thin-plate spline deformable model. In: 2015 3rd RSI International Conference on Robotics and Mechatronics (ICROM). pp. 743–748. IEEE (2015)
27. Vercauteren, T., Pennec, X., Perchant, A., Ayache, N.: Non-parametric diffeomorphic image registration with the demons algorithm. In: International Conference on Medical Image Computing and Computer-Assisted Intervention. pp. 319–326. Springer (2007)
28. de Vos, B.D., Berendsen, F.F., Viergever, M.A., Staring, M., Išgum, I.: End-to-end unsupervised deformable image registration with a convolutional neural network. In: Deep Learning in Medical Image Analysis and Multimodal Learning for Clinical Decision Support, pp. 204–212. Springer (2017)
29. Xu, Y., Sun, B.: Color-compensated multi-scale exposure fusion based on physical features. *Optik* **223**, 165494 (2020)
30. Xu, Y., Sun, B., Yan, X., Hu, J., Chen, M.: Multi-focus image fusion using learning based matting with sum of the gaussian-based modified laplacian. *Digital Signal Processing* **106**, 102821 (2020)
31. Xu, Y., Yang, C., Sun, B., Yan, X., Chen, M.: A novel multi-scale fusion framework for detail-preserving low-light image enhancement. *Information Sciences* **548**, 378–397 (2021)
32. Yan, X., Liu, Y., Xu, Y., Jia, M.: Multistep forecasting for diurnal wind speed based on hybrid deep learning model with improved singular spectrum decomposition. *Energy Conversion and Management* **225**, 113456 (2020)
33. Yang, X., Kwitt, R., Styner, M., Niethammer, M.: Quicksilver: Fast predictive image registration—a deep learning approach. *NeuroImage* **158**, 378–396 (2017)
34. Zachiu, C., Papadakis, N., Ries, M., Moonen, C., de Senneville, B.D.: An improved optical flow tracking technique for real-time **mr**-guided beam therapies in moving organs. *Physics in Medicine & Biology* **60**(23), 9003 (2015)